4.5 Rotating Gravity Currents

When relatively fresh river or estuary water discharges into the open ocean, it tends to turn to the (Northern Hemisphere) right and form a coastal surface flow or 'gravity current' (e.g. Munchow and Garvine 1993 and Rennie, et al. 1999). The outflow can be modulated, and sometimes blocked, by upwelling-favorable winds blowing across the mouth of the estuary. This is the case when northeastward winds blow across the mouth of Chesapeake Bay. When the winds relax or change direction, the brackish surface layer that normally resides in the bay is released. It exits and flows southwestward in a gravity current or plume along the Virginia and N. Carolina coasts (Figure 4.5.1). The leading edge of the current forms a blunt nose that can sometimes be seen at the free surface from the shoreline (Figure 4.5.2). A similar phenomenon occurs in the now familiar California coastal atmospheric marine layer (Beardsley et al. 1987 and Dorman 1987). At the beginning of the event shown in Figure I2b, the winds are from the north and the marine layer is gathered offshore of the Southern California Bight. At the time the image was taken, the marine layer has surged northward in response to a wind reversal. The leading edge can be seen near Point Arena, where it has stalled, formed an eddy, and resumed its northward travel.

The nonrotating gravity current has been studied extensively (Simson, 1997) and many of the ideas developed in this body of work form the basis for models with rotation. other sources of ideas for rotating gravity currents are early laboratory experiments, including Stern et al. 1982, Griffiths and Hopfinger 1983, Kubokawa and Hanawa 1984b, and more recently, Helfrich and Mullarney 2006. In these experiments, a homogeneous layer floating on an ambient fluid of slightly greater density and held in a reservoir is released and allowed to flow into a rotating channel or annulus. The situation is similar in some respects to the full dam break problem considered in Section 3.3, but turned upside down. The contact with the free surface avoids some of the frictional complications that would occur if the intrusion rubbed against the bottom. The fluid seeks out the right-hand wall of the channel and forms a boundary current, but unlike the thin-nose found in the single-layer version of the problem (Figure 3.3.3), the two-layer gravity current forms a blunt nose. This feature is evident in Figure 4.5.2 and in a sequence of realizations of a laboratory current (Figure 4.5.3). The upper image in each pair is a plan view, while the lower image is a side view created by a mirror reflection. Lateral and vertical detrainment of the (dyed, fresh) fluid in the current into the (clear, saline) ambient fluid can be observed, particularly in the early stages. In the four laboratory experiments cited, the nose is observed to propagate at the speed

$$c_b{}^* = \beta (g' d_b{}^*)^{1/2}, \qquad (4.5.1)$$

where $d_b{}^*$ is the upper layer depth at the wall, just upstream of the head (Figure 4.5.4) and β ranges over 1.0-1.3. The width $w_b{}^*$ of the current behind the head is more difficult to define due to the presence of eddies and billows around the outer edge. Nevertheless all investigations show that, regardless of definition,

$$w_p* = \beta_w \sqrt{g'd_b*} / f ,$$

with $0.5 < \beta_w < 0.8$. The values of c_b*, d_b* and w_b* tend to decrease gradually with time. In some experiments the leading edge stagnates, creating an expanding gyre behind the leading edge. The traditional view (Figure 4.5.4) is that the gravity current consists of a blunt nose followed by a relatively thick 'head' region, a thinner 'neck', and a long and gradually thickening rear portion that joins to the reservoir. In some cases the neck and head can be distinguished only in the early stages of the experiment. If drifting particles are placed in the flow it is observed that the head is fed from the rear by a relatively laminar current near the wall. Upon reaching the blunt nose, some of this fluid is diverted offshore where it reverses direction and moves upstream relative to the nose, possibly becoming detrained. The basic elements of this circulation are shown in a numerical simulation of the current at an early stage (Figure 4.5.5). The positive flow that feeds the head lies between the (dashed) $v*=c_b*$ contour and the wall. The velocity vectors are plotted in a frame of reference translating at speed c_b*, so the positive flow feeding the head appears weak. Retrograde motion is observed along the offshore portion of the intrusion.

Various attempts have been made to predict c_b* in terms of the properties of the flow just upstream of the head. Although the turbulent character of the current makes it difficult to find properties that are conserved between the nose and upstream, this problem can be circumvented by restricting attention to the leading edge of the nose and along the wall, where the unsteadiness and turbulence is observed to be minimal. Consider a side view of an idealized version of the current in a frame of reference translating at speed c_b* (Figure 4.5.6). The tip s of the nose is a stagnation point and the denser fluid approaches from the far right a at speed c_b*. The Bernoulli function evaluated at the free surface (where the pressure is considered zero) is

$$B* = \frac{u*^2 + v_m*^2}{2} - fc_b* \, x* + g\eta*, \qquad (4.5.2)$$

where $v_m* = v* - c_b*$ is the y-velocity seen in the moving frame. (The factor fc_b*x* accounts for the moving reference frame and g represents full gravity.) Assuming that $B*$ is conserved along the wall streamline that connects a to s, (4.5.2) reduces to $g\eta_s* = c_b*^2 /2$, where η_s* is the free surface elevation at the stagnation point and η_a* has been set to zero. It is further assumed that the wall flow remains steady between the nose and an upstream location b where the depth and velocity are approximately uniform. Conservation of $B*$ between s and b leads to $\frac{1}{2}(v_b* - c_b*)^2 + g\eta_b* = g\eta_s* = \frac{1}{2}c_b*^2$ if the previous relation is used. To this point, no restriction on the dynamics of the denser fluid has been made. However, if this denser fluid is considered dynamically inactive, then the relation $g\eta* = g'd*$ can be invoked, leading to $\frac{1}{2}(v_b* - c_b*)^2 + g'd_b* = \frac{1}{2}c_b*^2$, or

$$c_b* = \tfrac{1}{2}v_b* + g'd_b*/v_b*. \qquad (4.5.3)$$

By minimizing c_b^* over positive v_b^* it can easily be shown that $c_b^* \geq (2g'd_{-\infty}^*)^{1/2}$. The lower bound is actually achieved in the nonrotating version of the dam break, where v and d become independent of x. If no detrainment into the lower layer occurs and the plume remains in a steady state, v_b must equal c_b and (3) reduces to the lower bound

$$c_b = (2g'd_b)^{1/2} \qquad (4.5.4)$$

(Benjamin, 1968); that is, $\beta = 2^{1/2}$. Thus, rotation generally increases the speed of the bore if the latter is scaled by $(g'd_b^*)^{1/2}$, a prediction that is in general agreement with laboratory observations. However, as already mentioned, the experimental values of β tend to fall below $2^{1/2}$. This failure has been attributed to various causes, including the presence of friction (Martin and Lane-Serff, 2005; Helfrich and Mullarney, 2006;) and the participation of the lower layer (Benjamin 1968 and Klemp et al. 1994 and 1997, Hacker and Linden 2005, Martin et al. 2005.)

If the entire gravity current head is regarded as steady, a second constraint exists in the form of conservation of the volume flux. In the moving reference frame the volume flux at any section of the current must be zero. Applying this restriction at the section $y^* = y_b^*$ that coincides with point b in Figure 4.5.6b leads to

$$\int_0^{-w_b^*} (d^* v_m^*) dx^* = \int_0^{-w_b^*} [d^*(v^* - c_b^*)] dx^* = 0$$

or

$$Q_b^* = c_b^* A_b^*, \qquad (4.5.5)$$

where $Q_b^* = \int_0^{-w_2^*} (d^* v^*)_{y^*=y_b^*} dx^*$ is the rest frame volume transport at b and

$A_b^* = \int_0^{-w_b^*} (d^*)_{y^*=y_b^*} dx^*$ is the cross section area there. By assumption, the flow is uniform at y_b and therefore geostrophically balanced. Thus

$$g'd_b^{*2} = fc_b^* A_b^*. \qquad (4.5.6).$$

The relation (4.5.6) ads the new variable A_b^* to the mix and further information is required in order to close the problem for c_b^*. One approach is to assume that the current has uniform potential vorticity, which occurs if the source reservoir has constant depth and friction and entrainment are absent. The uniform potential vorticity depth profile (2.3.1) allows one to write A_b^* in terms of v_b^* and d_b^*, thus closing the system (4.5.4) and (4.5.6). Kubokawa and Hanawa 1984b and later Helfrich and Mullarney used equivalent approaches and found c_b^* to be of the form (4.5.1), but with β only marginally greater than $2^{1/2}$. The corresponding $\beta_w = 0.78$.

Yet another theory for the nose speed is due to Nof (1987) with later refinements by Hacker and Linden (2002), who added a third constraint of momentum conservation and applied it to a model in which the gravity current has no flow relative to the front (i.e. $v^*(x^*, y^*) = c_b^*$) The resulting $\beta = 2^{1/2}$ is identical to the result for no rotation and $\beta_w = 2^{-1/2}$.

Attention to this point has been focused on the local properties of the gravity current near its leading edge. It still remains to relate v_b^* and d_b^* to the reservoir conditions. Assuming that the flow to the rear of the head varies gradually with y^*, it is reasonable to apply semigeostrophic theory and use the method of characteristics to link the head to the reservoir. One way of proceeding is to calculate the solution to a dam break problem as in Section 3.3. Although one could in principle perform this calculation for a full two-layer system, the solution is complicated by the presence of a lower layer potential vorticity front that initially lies at the position of the barrier (where the lower layer thickness is discontinuous). When the barrier is removed this front is overridden by the upper layer gravity current and must be accounted for. The problem is avoided if the lower layer is considered infinitely deep, for then the solution proceeds as described in Section 3.3. As before, the problem is considerably simplified if one of the Riemann invariants R_+ or R_- is constant for the initial condition as a whole. Stern et al. (1982) opted for constant R_- since this produces a steepening flow that results in the formation of a blunt nose. The requirement that the nose be blunt leads to the identification of a unique value of R_- (see Exercise 1) and allows closure of the problem. The resulting current evolves into a uniform flow with width corresponding to $\beta_w = 0.42$. At the leading edge of the current is a shock that is interpreted as the nose. Energy conservation in the form of (4.5.3) is assumed to hold across the shock and this is sufficient to determine the nose speed coefficient $\beta = 1.57$. The solution is elegant in that the detrainment rate (32%) can be predicted. Kubokawa and Hanawa (1984b) altered this approach by relaxing the requirement that R_- be consistent with a smooth, blunt nose. The missing constraint is instead provided by a requirement of conservation of volume transport (4.5.6) across the nose. The resulting solution therefore has no detrainment.

Both of the solutions are subject to the objection raised in Sections 1.3 and 3.3, namely that negative v occurs at the position of the barrier at the instant of its removal. The alternative is to consider R_+ uniform, as is done in the traditional dam break. If this approach were to be carried to its logical conclusion, the result would be a rarefying intrusion with a thin leading edge (as in Figure 3.3.3). The blunt nose that is actually observed in the two-layer system might, however, be explainable as a local feature, created by processes that tend to hinder the leading edge. Clarification and guidance can be gained from a peculiar version of the dam break problem with zero rotation. Suppose that instead of being removed altogether, the initial barrier is moved horizontally at a fixed speed $< 2(g'd_o^*)^{1/2}$ away from the reservoir. Then as shown by Stoker 1957 (also see Exercise 5 of Section 1.3) the flow near the moving barrier consists of a slab-like region with constant depth and velocity. This region extends upstream from the barrier and joins with a second, rarefying region. The structure of the second region is the same as in the classical dam break. Abbott (1961) and Garvine (1981) used this piecewise continuous solution, interpreting the slab region is a model of the head and taking $(2g'd_b^*)^{1/2}$ as the barrier speed. Helfrich and Mullarney (2004) have taken a similar

view of the rotating gravity current in a channel (Figure 4.5.6b). The head consists of a translating slab with width w_b^* and velocity c_b^*. The slab-like head, which has width w_b^* and velocity c_b^*, is joined to a rarefying feeder current that extends from the rear of the head back into the reservoir. The feeder current is just a truncated version of the rarefying intrusion shown in Figure 3.13a. It becomes attached to the left sidewall at an upstream point y_{sep}^*. At the point of transition $y_a^*(t^*)$ between the head and feeder current, the volume transport and width are required to be continuous. Continuity of transport implies that the head suffers no detrainment. Under the constraint of uniform R_+ each width value w_e within the separated portion of the rarefying intrusion travels at a characteristic speed c_-^* that depends only on the local width. The transition point $y_a^*(t^*)$ therefore travels at the characteristic speed $c_-^*(w_b^*)$.

In order to complete the solution, a separate model for the nose speed c_b^* must be used. The model takes the form (1) with the value of β given empirically or by one of the above theories. It turns out that $dy_a^*/dt^* < c_b^*$ regardless of this choice and the transition point therefore recedes relative to the nose. The value of w_b itself is determined by the requirement of continuity of volume transport. As shown by Helfrich and Mullarney (2006), the general procedure can be carried out for non-separated gravity currents in a channel, as generally occurs for dimensionless channel width $w = w^*/(g'd_{1\infty}^*)^{1/2}$ less than about 0.5 in the experiments. The resulting model allows properties like c_b^*, c_{sep}^*, w_b^* and h_b^* to be related to w^*.

A comparison is made (Figure 4.5.7) between the predicted values, all based on a nominal empirical value $\beta=1.2$, and data from the Stern et al. (1982) and Helfrich and Mullarney (2006) experiments. In browsing through this figure the reader will find significant discrepancies between the two sets of experimental data, despite the similarity between the two experiments. Some of these differences may be due to varying definitions of variables or the way they are measured. For example, the experimental values of c_b^* are generally observed to suffer a slow decrease with time, probably due to frictional effects, and discrepancies in measured values of c_b^* may be due to the time at which the measurements were taken. Also the theory in this case is not completely pure since it is based on an empirical β. Nevertheless, the comparison indicates some success in the prediction of values or trends for certain quantities such as c_b^*, c_{sep}^*, w_b^*; the prediction for h_b^* is less successful.

The foremost shortcoming in the theory or rotating gravity currents is failure to adequately address the entrainment problem. Only the theory of Stern et al. (1982) offers a prediction of entrainment. At the time of this writing there exist no laboratory measurements of entrainment against which this theory can be compared. It may also seem odd to the reader that surface gravity current doctrine emphasizes detrainment of fluid into the ambient fluid whereas the literature on descending plumes (section 2.12) emphasized entrainment of ambient fluid. To some extent, the difference between entrainment and detrainment is based on how the current and ambient fluid are defined. But, as pointed out by McClimans (1994), different turbulent regimes naturally lead to different categorizations. For example, a surface gravity current that has a non-turbulent and undiluted core region and whose turbulence exists only near the outer edge, may naturally be regarded as detraining. On the other hand, a descending plume that

experiences turbulence over its entire cross-section, with consequent dilution of density, may naturally be regarded as entraining.

Exercises

1. *The gravity current as a steepening bore*. Following Stern et al. (1982), consider the curves of constant Riemann invariant for separated, zero-potential vorticity flow (Figure 2.5). (They considered finite but constant potential vorticity and the diagram for this case is similar to Figure 2.5.) As a model of a gravity current we seek a solution that has R_- =constant and that allows a blunt 'nose' (i.e. permits w_e to go to zero while $\partial w_e / \partial y$ remains finite). Of all the candidate R_-=constant curves in Figure 2.5 that have this property, show that only the curve that intersects the origin is consistent with a blunt nose. (Hint: one approach is to use equations (2.3.19).

1. *A bound on the gravity current width.*

   (a) Suppose that the gravity current is considered steady in a frame of reference moving with the nose speed c_b and that the width approaches a uniform value w_b upstream of the nose. By applying the Bernoulli equation between the nose (point s in Figure 4.5.6a) and an upstream point on the outer edge (e in the same figure) show that $w_b* \leq c_b*/2f$. (This result was first obtained by Stern et al. 1982.)

   (b) Show that the result is invalidated if an energy loss from s to p is permitted.

   (c) Show that the bound is equivalent to $\beta_w \leq \beta/2$.

Figure Captions

Figure 4.5.1 Synthetic aperture radar image showing a coastal gravity current flowing south out of the mouth of Chesapeake Bay. (From Donato and Marorino, 2002.)

Figure 4.5.2 Photo of nose of Chesapeake Bay plume near Duck, NC, March 1991. (Photo by William Birkemeier, US Army Corps of Engineers.)

Figure 4.5.3   Advancing gravity current as seen in plan and side views (upper and lower half of each frame) for successive times. The side view in each case is a mirror reflection. The photos are based on the laboratory experiments performed by Stern, et al. 1982.

Figure 4.5.4 Traditional view of a gravity current in a rotating channel.

Figure 4.5.5 Numerical solution showing the horizontal circulation in the head of a gravity current as seen by an observed moving with the speed c_b. The dashed curve corresponds to zero along-shore velocity in the moving frame. (From Helfrich and Mullarney, 2006).

Figure 4.5.6 Idealization of gravity current nose region.

Figure 4.5.7 Comparison of solutions for a semigeostrophic gravity current with uniform Reimann invariant R_+ with data from various laboratory and numerical simulations. The speeds shown have been nondimensionalized using $(g'd_{1\infty})^{1/2}$, where $d_{1\infty}$ is the initial depth in the reservoir for the upper layer. The widths w and w_b have been scaled by $(g'd_{1\infty})^{1/2}/f$ and d_b by $d_{1\infty}$. The theory, which is shown by solid curves in each frame, is based on a nose speed of the form (1) with the nominal empirical value $\beta=1.2$. The theory and some of the experiments extend into the range in which the gravity current does not separate from the left channel wall (roughly $w<0.5$). Triangles and squares represent data from the laboratory experiments of Helfich and Mullarney (2006) and Stern et al. (1982), respectively. Open and filled circles represent data from a numerical model (Helfrich and Mullarney, 2006) with no-slip and free-slip boundary conditions. In (a) c_b* and $c_{sep}*$ are both shown, though Stern et al. (1982) did not measure the latter. Frames (b) and (c) show comparisons based on the nose width and depth. (From Helfrich and Mullarney (2006), Figure 15.)
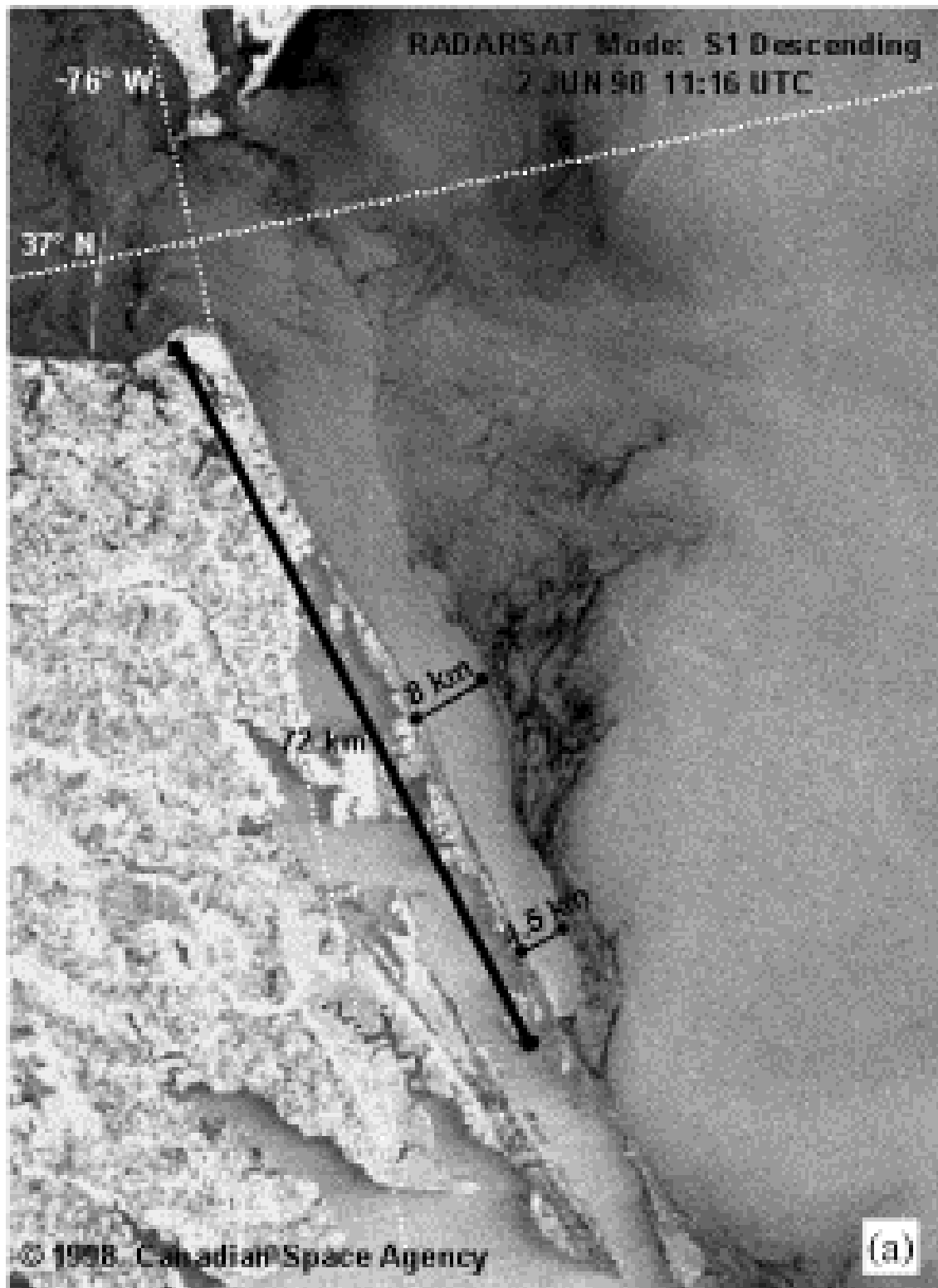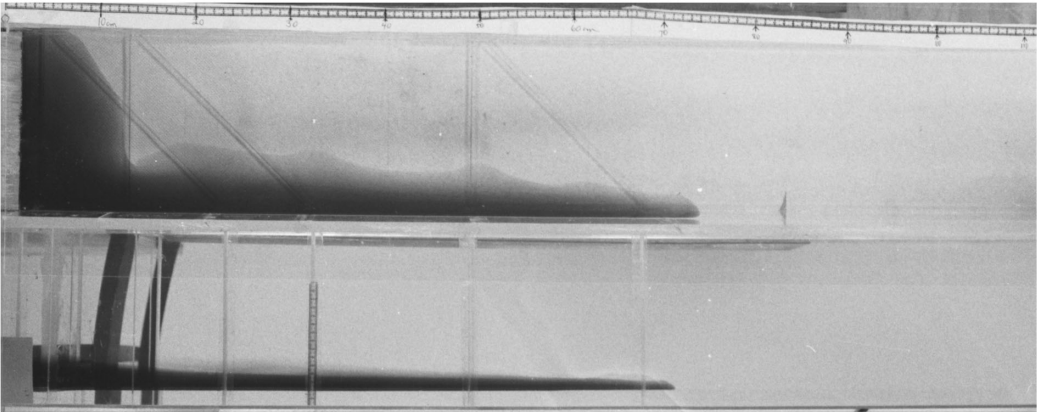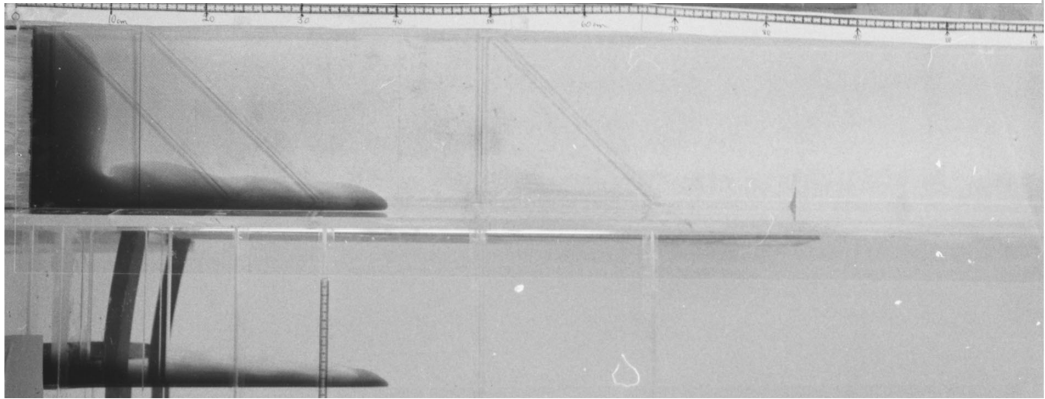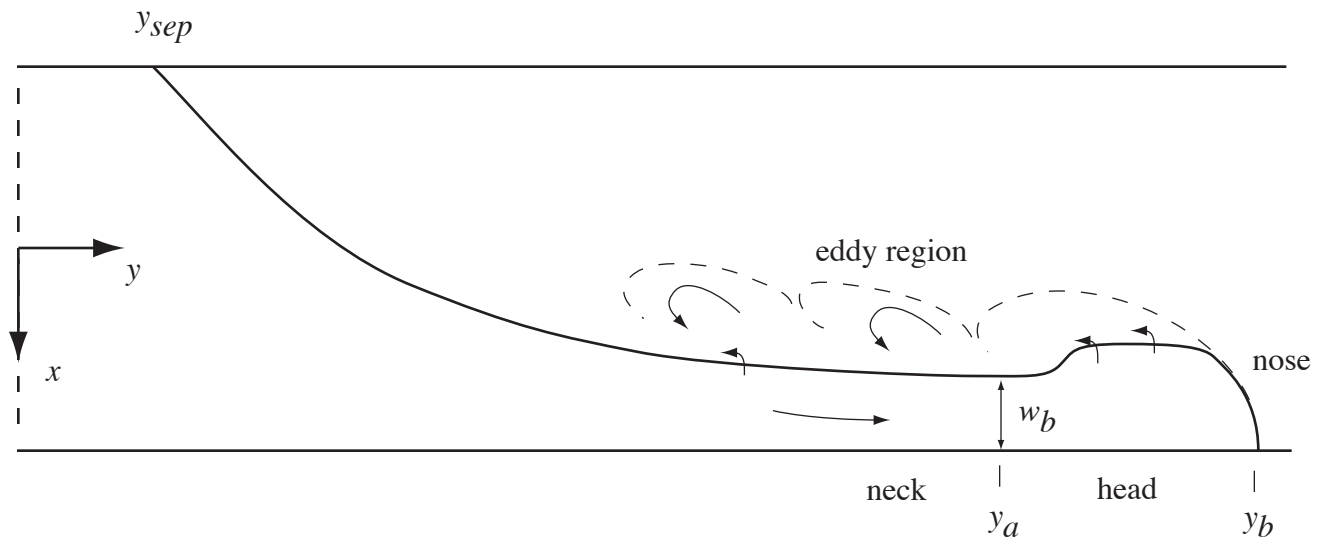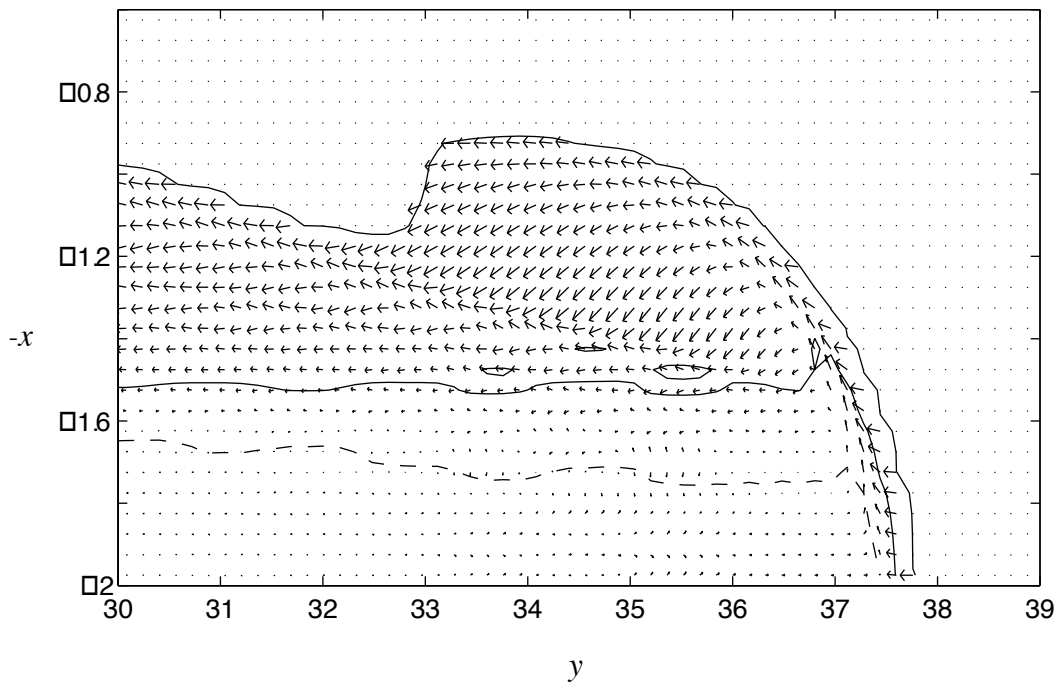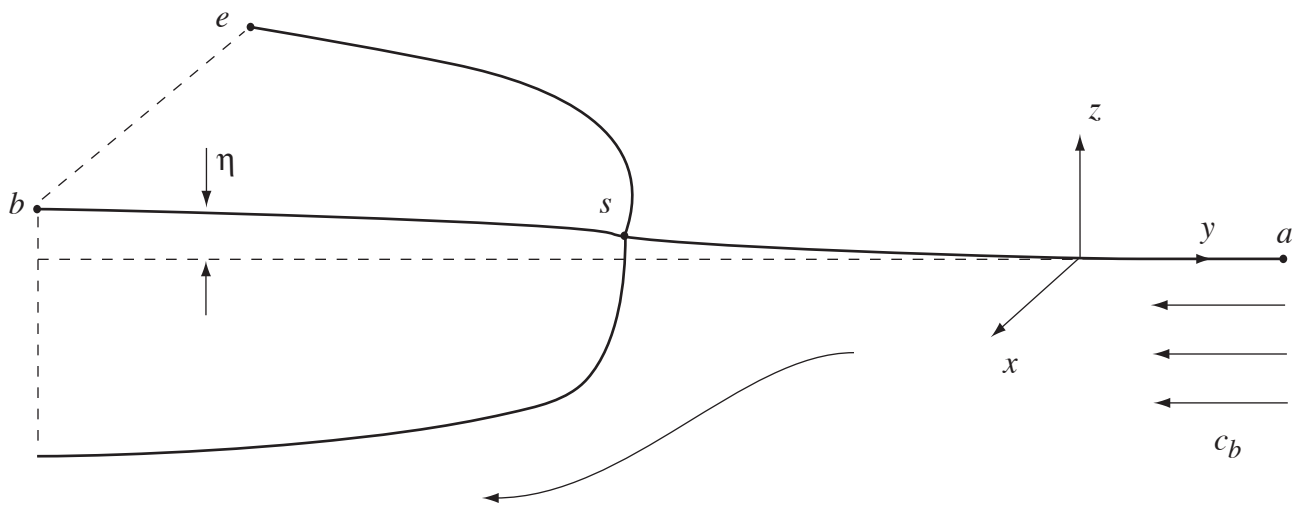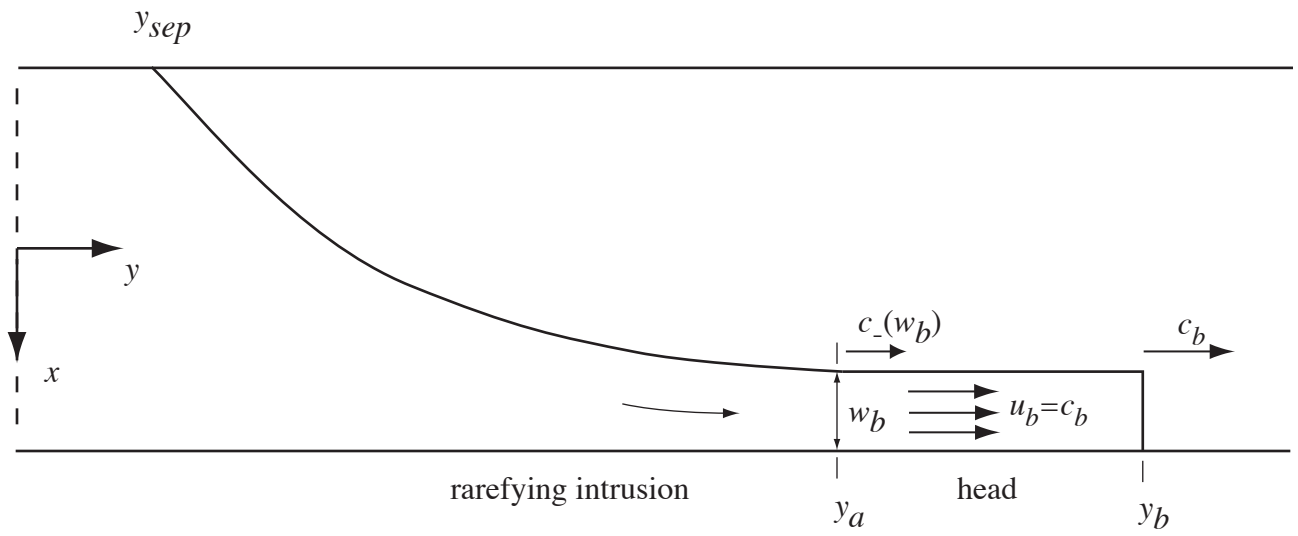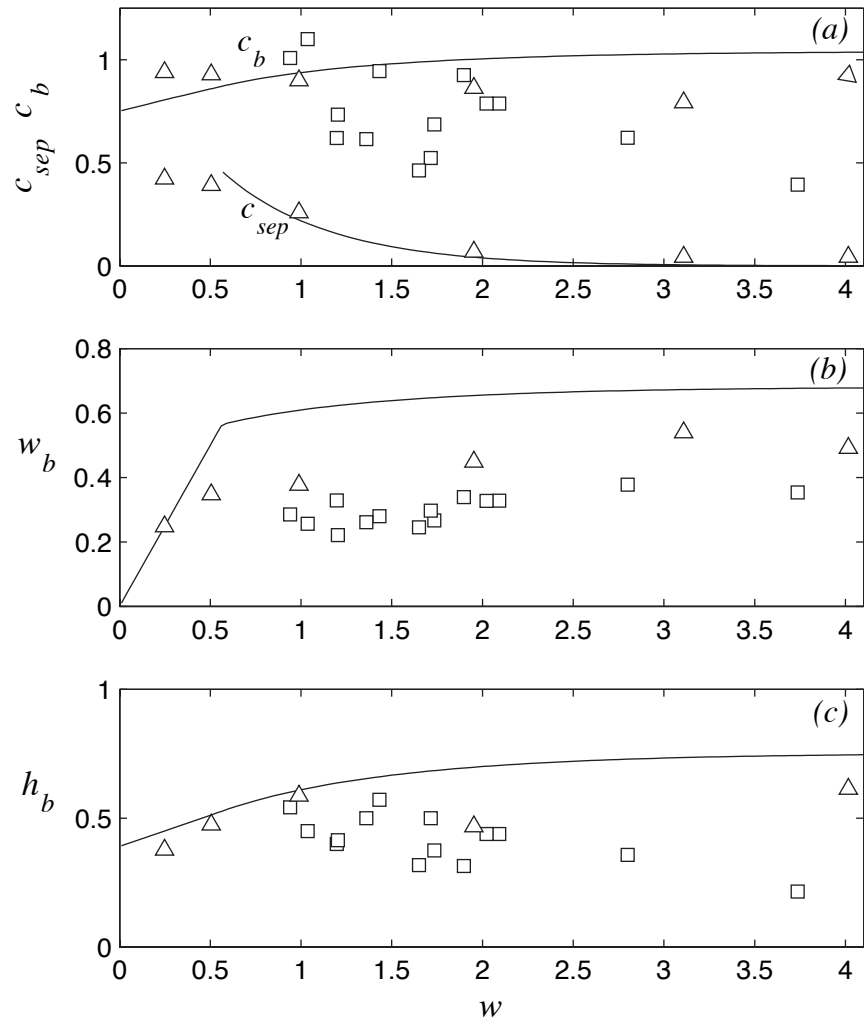
Fig. 4.5.1
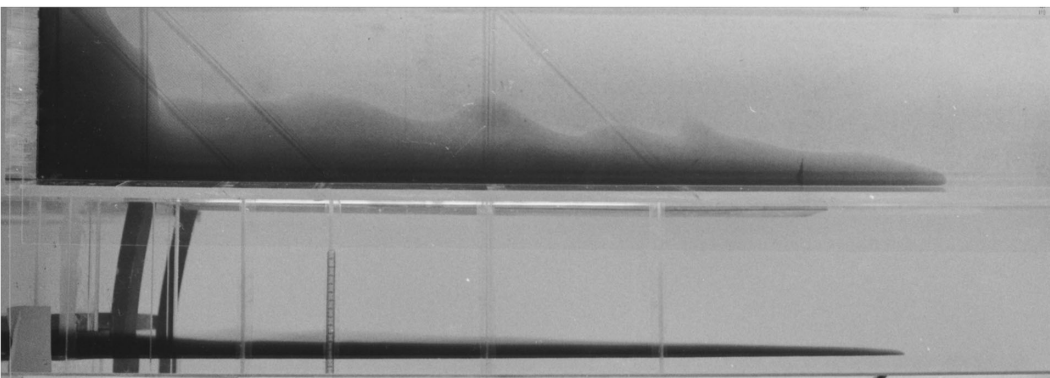
Figure 4.5.4

Figure 4.5.5

(a)

(b)

Figure 4.5.6

Figure 4.5.7